A LOW COST MACRO-MICRO POSITIONING SYSTEM WITH SMA-ACTUATED MICRO STAGE

Eric Ho, Systems Engineer, Honeywell Aerospace, Mississauga ON, Canada
Rob Gorbet, Assistant Professor, Dept. of ECE, University of Waterloo, Waterloo ON, Canada
Contact: rbgorbet@uwaterloo.ca

Received August 2006, Accepted December 2006
No. 06-CSME-42, E.I.C. Accession 2961

ABSTRACT

Macro-micro systems allow high-resolution positioning over greater ranges of operation that would be achievable with precision positioning systems. Piezoceramic actuators have established themselves as the principle technology for commercial micro-positioning applications, and the trend in research is to push the limits of resolution down to the nanometer and sub-nanometer scales. Other smart materials offer the potential for lightweight, continuous actuation over small ranges, and hence may be useful in micro-positioning applications. This work focuses on the potential for SMA actuators to enable low-cost micro-positioning. Compared to piezos, SMA offer longer range and lower actuation voltages, enabling lower-cost drive electronics and removing the need for costly precision mechanical amplification stages. A prototype single-axis macro-micro positioning system is described, with a macro range of 200 mm and relative positioning precision of better than 5 μm. The micro stage is driven by an NM70 SMA actuator from NanoMuscle. Macro and micro stages are modelled and controllers developed, and experimental system performance is evaluated. The success of the system provides an inexpensive platform for the study of macro-micro positioning issues such as stage coupling, friction, and drive flexibility, as well as for the position control of SMA.

UN SYSTÈME DE POSITIONNEMENT 'MACRO-MICRO' A COUT FAIBLE COMPORTANT UN ACTIONNEUR AMF

RÉSUMÉ

Les manipulateurs "Macro-micro" permettent une opération précise avec une aire de travail plus importante comparée à un simple positionneur haute-précision. Les actionneurs piezocéramiques sont depuis longtemps le choix principal chez les actionneurs à micro-précision, et la direction générale de la recherche est de vouloir augmenter la résolution de ces actionneurs vers des précisions en dessous du nanomètre. En plus des piezocéramiques, d'autres matériaux dit 'intelligents' sont adaptés à la conception d'actionneurs linéaires et légers, avec une haute précision dans une plage d'action limitée. Cet article examine en particulier les alliages à mémoire de forme (AMF) et les possibilités que ceux-ci peuvent offrir dans le domaine du micro-positionnement à cout faible. Par rapport aux piezocéramiques, les AMF offrent une plage d'action plus importante et nécessitent une plus faible tension électrique. Ceci permet de réduire le cout de l'électronique associée ainsi que d'éliminer les plateformes d'amplification mécanique. Nous décrivons un manipulateur 'macro-micro' prototype, possédant un axe de déplacement, avec une plage d'opération de 200 mm et une précision relative supérieure à 5 μm. Le micro-positionneur est composé d'un actionneur AMF NM70 fabriqué par NanoMuscle. La modélisation est décrite pour les deux actionneurs du prototype, macro et micro. Le développement des contrôleurs et une évaluation de la performance du système sont aussi présentés. Le prototype représente un système à cout faible permettant la continuation de notre recherche dans les domaines associés : le couplage entre les plateformes macro et micro, l'effet du frottement, les vibrations, et le contrôle précis des actionneurs AMF.

INTRODUCTION

The decreasing size of electronic circuits has contributed greatly to the development of micron and sub-micron scale manufacturing techniques. One development often employed in micro-automation is the coupling of a fine (micro) and coarse (macro) manipulator to provide micro-scale processing over a large workspace. This allows both for transport of a part or tool over large distances, and high precision processing via the fine manipulator. Piezoelectric ceramics (piezos) and piezo-based actuators currently dominate as the actuation device for micron and sub-micron scale positioning. Piezos generate high forces and high stiffness but are only capable of microstrain displacements, and are thus well-suited to sub-micron positioning with limited range. Indeed, piezo actuators are now available for sub-nanometer positioning. Precision flexure guides are often used for mechanical amplification and trajectory constraint when greater range is required. However, this increases the cost of the actuator due to the complex design and wire EDM machining typically required for complicated flexures. A single-axis micro-positioner with integrated sensing can cost several thousand dollars[1]. Another piezo-based alternative are the so-called Inchworm motors, which can theoretically provide unlimited high-precision travel, although available commercial systems are limited to 50mm[2]. Again, complicated mechanical construction and control requirements make these actuators quite expensive.

With the focus of precision positioning research moving into the nanometer scale and beyond, the goal of this work is to investigate possibilities for low-cost positioning at micron precision. Shape memory alloys (SMAs) may offer a viable alternative to piezos in positioning applications with such precision requirements, at a fraction of the cost. Since SMAs naturally have greater stroke than piezos and generate sufficient force for many applications, actuators can be coupled directly to the end-effector on the micro stage without the need for complex mechanical amplification. The greater stroke and low mass of SMA reduce the need for macro-stage power and stiffness. In applications where precision is required only relative to macro-stage location, the need for macro-stage precision is also reduced. SMAs can also be driven with much lower voltages than piezos, eliminating the need for step-up converters and power conditioning. The primary drawback of SMA actuators in this type of application is the limited bandwidth achievable, typically on the order of 1 Hz, due to the thermal nature of the enabling transformation.

The goal of this paper is to present experimental results demonstrating the construction of a low-cost (<$300) single-axis macro-micro positioning system with a range of 200mm and a relative positioning resolution of less than 5 μm. Potential applications are those where bandwidth and absolute positioning are not critical, for example low-speed visual inspection relative to a local fiducial mark. The micro stage incorporates a NanoMuscle SMA actuator. The following section of the paper describes the prototype, including macro and micro stage actuators and feedback sensor design. In the next section, simulation models are developed and validated for both the macro and micro stage, while the final section describes the closed-loop controllers that were designed. Performance is evaluated both in simulation and experimentally, with good agreement between the two.

EXPERIMENTAL PROTOTYPE

The experimental system comprises a modified printer carriage to provide long range, macro-scale linear motion (approximately 200 mm range and 50 μm precision) and a micro-scale system

(approximately 4 mm range and 5 μm target precision) that uses a NanoMuscle SMA-based actuator mounted on the print head platform. Both components are monitored and controlled by Simulink via Matlab's Real Time Workshop and a MultiQ-3 data acquisition board (MQ3) manufactured by Quanser Consulting. The overall system is shown in Figure 1.

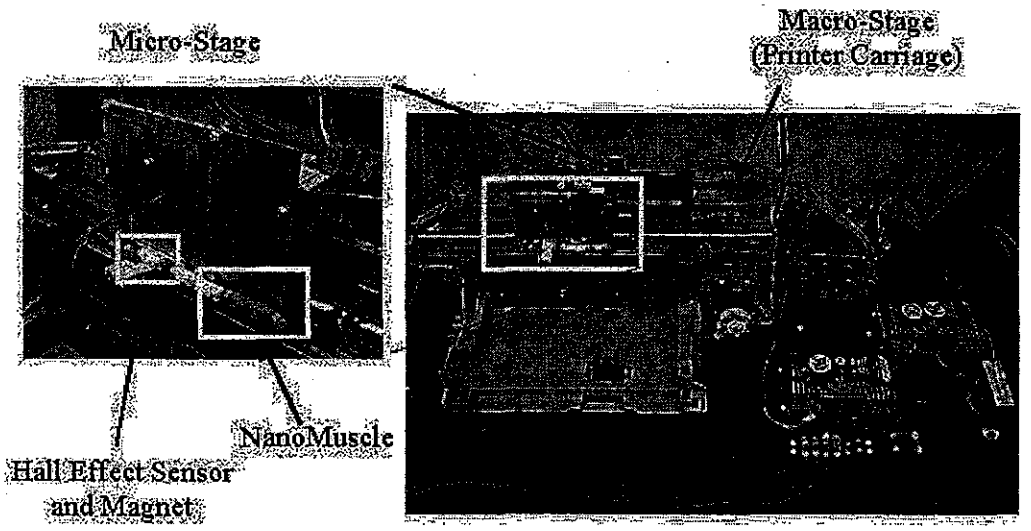

Figure 1: Prototype Positioning System

Macro-Stage Description

The macro stage consists of an ink-jet printer modified to interface with the MultiQ-3 D/A board and to accommodate the mounting of the micro stage on the printer carriage. The carriage drive DC motor is controlled using pulse width modulation (PWM) with an amplitude of 20 V and a duty cycle tuned to 0 - 100 % for a 0 - 5 V analog output from the MQ3 board. Position feedback is provided by a linear encoder with a resolution of 50 μm resolution, already incorporated in the printer.

Micro-Stage Design

The micro stage consists of a NanoMuscle NM70 SMA actuator in series with a linear flexure guide and a bias spring. Feedback is provided via a Hall effect sensor and magnets. A CAD illustration of the micro stage is shown in Figure 2 (Hall effect sensor not shown).

The NanoMuscle NM70 (see Figure 3a) consists of a series of alternating metal plates and SMA wires arranged electrically in series and mechanically in parallel, as shown in Figure 3b. The top metal plate is fixed while the bottom is attached to a load, and mechanical stops prevent wire over-strain. When the SMA wire is cool, the bias spring in Figure 2 fully extends the actuator. When current is run through the actuator, the wires contract. Each wire pulls a plate by a distance δ relative to the plate above it and this displacement is multiplied by the parallel plates. For the NM70, the total stroke $\Delta \approx 4\,\text{mm}$.

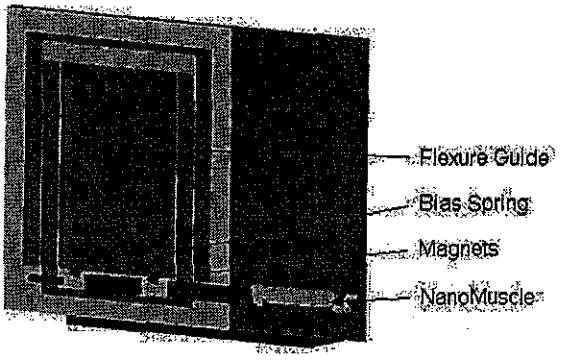

Figure 2: CAD Illustration of Micro Stage

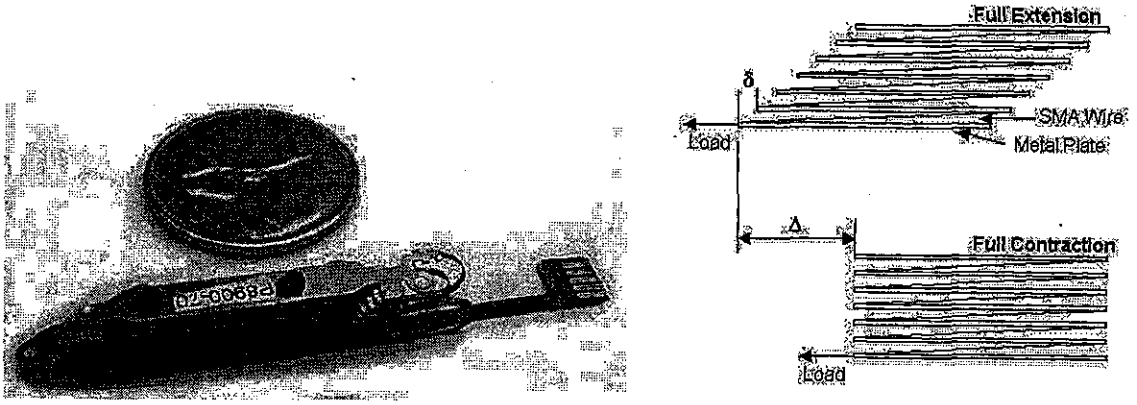

(a) (b)

Figure 3: (a) Photograph and (b) Schematic Illustration of Operation of the NanoMuscle Linear Actuator

The NM70 has a fully-integrated and proprietary digital interface, including logic signals corresponding to the end stops, over-current protection, and a digital CTRL input. CTRL is driven by a 20 V PWM signal with the duty cycle tuned to 0 - 20 % for a 0 - 5 V analog output from the MQ3 board, as recommended in [3].

To couple the micro stage actuator to the micro-platform, a guiding stage is required to support position feedback sensors and any future tools (such as a CCD inspection camera), and to ensure linear motion is maintained during operation. In order to introduce minimal friction in the system from this guide, a simple aluminum linear flexure guide was designed. The flexure is a set of four mechanically coupled cantilever beams machined using standard techniques in a sheet of 2 mm aluminum, and designed to accommodate the 4 mm displacement given the force range of the NM70 actuator. The opposing cantilever beam design guarantees motion along a single axis. Further details on the design of such structures can be found in [4].

Position feedback for the micro stage is provided by a Hall effect sensor combining the desirable qualities of light weight, small size, low cost, and non-contact measurement. The Hall effect sensor measures the magnetic flux from permanent magnets mounted on the moving flexure platform. Bipolar slide-by operation is used, where two magnets of opposite polarities are mounted beside each other forming a relatively linear flux profile similar to that of Figure 4. As the magnets slide by the fixed sensor, the flux profile seen by the sensor changes and this is reflected in the sensor output voltage.

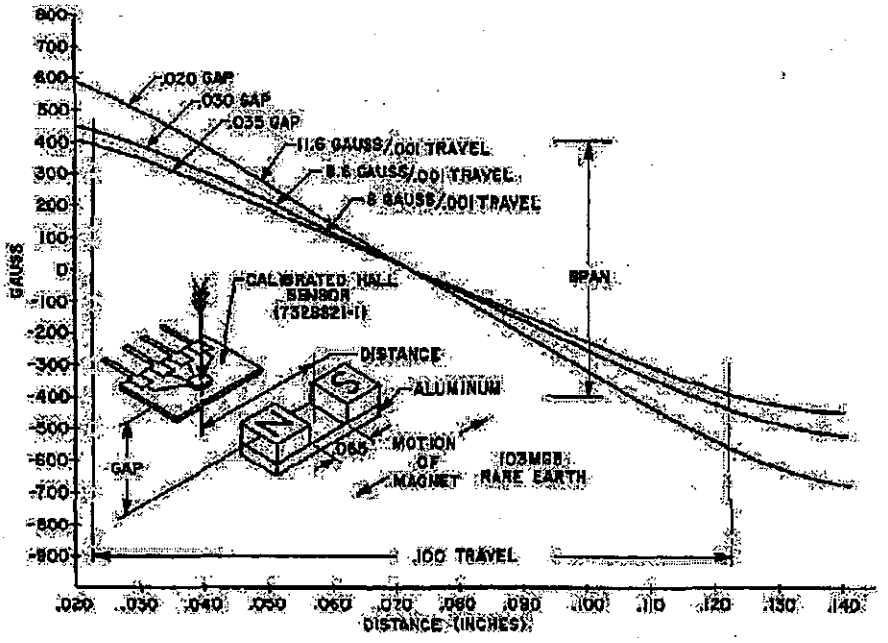

Figure 4: Flux Profile of Honeywell 103MG5 Magnet in Bipolar Slide-by Operation [5]

Pressed samarium cobalt cylinder magnets (Dexter Magnets, PR28CO120B) with a diameter of 3 mm and length of 2.5 mm were used. In their final configuration, these magnets provide a magnetic flux distribution of approximately 5 μm/Gauss over the range of 4 mm of micro stage motion.

A Honeywell SS94B1 Hall effect sensor with a sensitivity of 3.125 mV/Gauss was used to measure the magnetic flux variation during motion. Combining these sensitivities with the 12-bit resolution of the MQ3 D/A channel over the 0 - 5 V input range gives a theoretical measurement resolution of

$$5\ \left[\frac{\mu\text{m}}{\text{Gauss}}\right] \times \frac{1}{3.125}\ \left[\frac{\text{Gauss}}{\text{mV}}\right] \times \frac{5}{4096}\ \left[\frac{\text{V}}{\text{bit}}\right] = 1.953\ \left[\frac{\mu\text{m}}{\text{bit}}\right].$$

To mount the sensor and magnets to the micro stage, the magnets are press fit 4 mm apart into a small Teflon bar mounted onto the moving flexure platform. The sensor is mounted directly below the one of the magnets when the NanoMuscle is fully extended. When the actuator contracts, the magnets move until the other magnet lies above the sensor at full contraction, as shown in Figure 5.

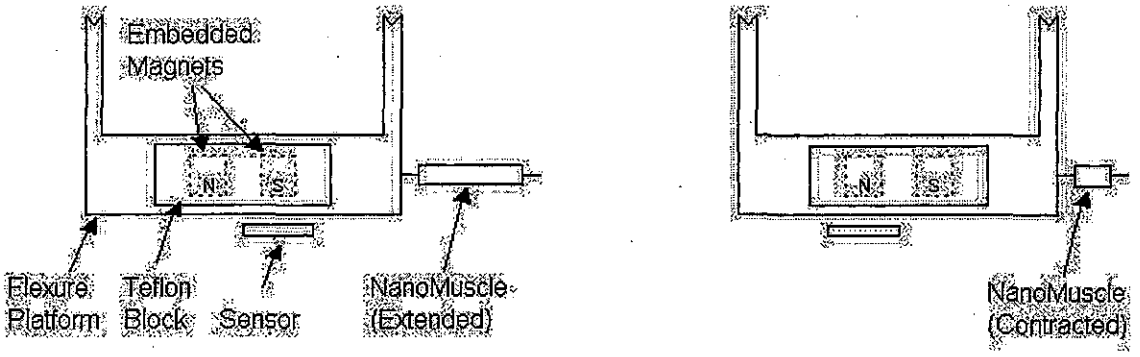

Figure 5: Illustration of the Micro-Stage Sensor System at Full (a) Extension and (b) Contraction

The vertical spacing of the magnets from the sensor is set experimentally by positioning each magnet to touch and thus saturate the sensor, which reads 2.5 V nominally, to either 0 V or 5 V. Each magnet is then raised to the point where the sensor is no longer saturated at either end of travel. To calibrate the sensor, an Agilent laser measurement system is used to measure the displacement of the micro stage. The calibration curve relating the Hall effect sensor reading to the actual position read by the laser is shown in Figure 6.

The approximate total cost of the micro stage, including feedback sensors and manufacturing costs of custom components, but not including drive and control electronics, is shown in Table 1. Note that NanoMuscle has ceased operations, and MIGA Motors (www.migamotors.com) has purchased the intellectual property and left-over stock of the NM70. The actuators are available from MIGA Motors at the listed price for quantities of 10, and are significantly cheaper in larger quantities. MIGA Motors also makes a similar product to the NanoMuscle.

SYSTEM MODELLING

In order to allow for off line controller design and the investigation of model-based controllers, mathematical open-loop modelling of the macro and micro stages is undertaken. For the macro stage, modified least squares (MLS) identification [6, e.g.] is applied after compensating for non-linearities identified in the system. In the case of the micro stage, a Preisach hysteresis model is

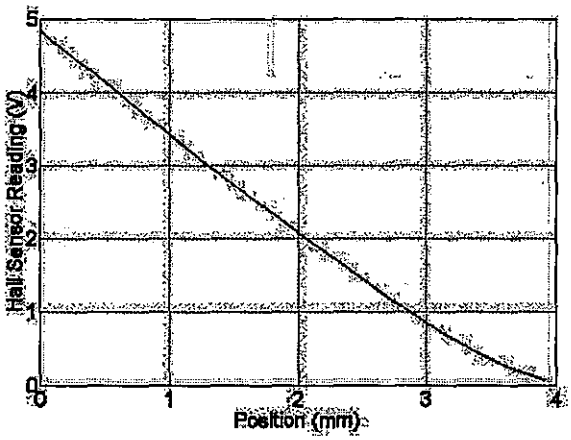

Figure 6: Position to Hall Effect Sensor Reading Relationship

Table 1: Approximate Cost Breakdown of Micro-Stage

Component	Approximate Cost ($ USD)
Hall Effect Sensor (Honeywell)	10
Magnets (Dexter)	5
Flexure Guide (in-house)	100
NM70 Actuator (NanoMuscle)	15
Magnet Mount (in-house)	20
NanoMuscle to Flexure Guide Linkage (in-house)	20
Bias Spring (in-house)	5
Total Cost	175

identified for the temperature-displacement behaviour of the NM70 SMA actuator. The Preisach model has been applied by a number of researchers to model smart material hysteresis, including shape memory alloys [7, 8, e.g.]. One appealing feature of the Preisach model is that is invertible and has a computationally efficient form[9]

Macro-Stage Modelling

The printer carriage system used for the macro stage is a mass sliding on a dry bushing, driven by a DC motor as illustrated schematically in Figure 7. Non-linearities occur due to control signal saturation as well as friction. It is assumed that the drive belt is sufficiently rigid that vibration due to drive flexibility can be neglected.

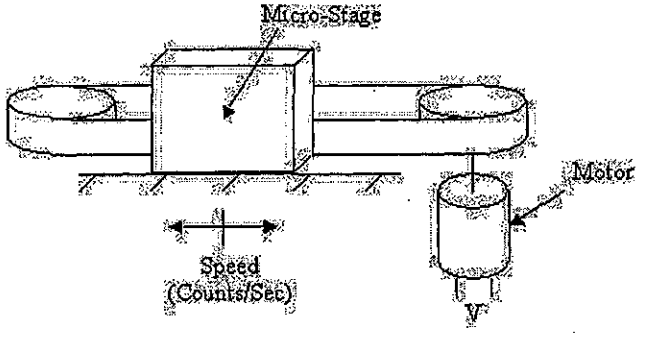

Figure 7: Schematic Illustration of the Macro Stage

The equation for electrical and mechanical dynamics of a DC motor are[10, e.g.]

$$L\frac{di}{dt} + Ri = K_a V - K_b \omega \tag{1}$$

$$J\frac{d\omega}{dt} + B\omega = K_t i \tag{2}$$

The electrical parameters L, R, and i are winding inductance, resistance, and current, K_b is a back-EMF constant, ω is angular velocity, K_a is an amplifier gain, and V is the amplifier input voltage. The mechanical parameters are J the inertia of the motor and payload, B a viscous damping coefficient, and K_t the motor torque constant. Assuming, as is generally the case, that the electrical system is much faster than the mechanical system (i.e., that $L \ll R$), and introducing a conversion factor K_{lin} from angular position to linear displacement $y = K_{lin}\omega$ gives

$$\frac{J}{K_{lin}}\dot{y} + \frac{B}{K_{lin}}y = \frac{K_t K_a}{R}V - \frac{K_t K_b}{RK_{lin}}y$$

$$\dot{y} + \frac{BR + K_t K_b}{JR}y = \frac{K_t K_a K_{lin}}{JR}V \tag{3}$$

Equation (3) has s-domain representation

$$\frac{Y(s)}{V(s)} = \frac{K_t K_a K_{lin}}{JRs + (BR + K_t K_b)},$$

and discretizing using a zero-order hold and a sampling rate of 1 kHz gives the discrete-domain transfer function

$$\frac{Y[z]}{V[z]} = \frac{b}{z+a} \tag{4}$$

where

$$\begin{aligned} a &= -e^{-[\frac{BR+K_tK_b}{JR}]T} \\ b &= -\frac{K_aK_{lin}K_t}{BR+K_tK_b}\left[e^{-[\frac{BR+K_tK_b}{JR}]T} - 1\right] \end{aligned}$$

Any viscous friction effects are assumed to be captured in the motor dynamics, and included in the damping coefficient B. The level of stiction and Coulomb friction are initially assumed equal, and their effects approximated as a dead zone in the control voltage. In order to apply linear system identification techniques, the dead zone model is characterized and then inverted in software prior to applying the identification signal. Figure 8 shows the linear motor model combined with the friction dead zone model, control signal saturation, and a discrete-time integrator to form the simulation model of the plant (inner box).

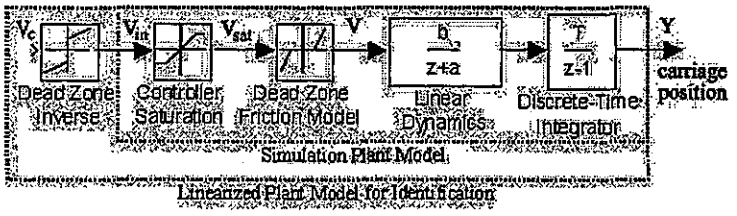

Figure 8: Block Diagram of the Open-Loop System with Initial Friction Model

To characterize the dead zone, progressively increasing DC voltages were applied to the prototype until smooth motion of the printer carriage was observed. The approximate threshold was measured to be 3 V, resulting in the dead zone friction model from the saturated control signal to the motor input shown in (5).

$$\begin{aligned} V &= \text{sgn}(V_{sat})(|V_{sat}| - 3), \quad |V_{sat}| \geq 3 \\ V &= 0, \quad |V_{sat}| < 0 \end{aligned} \tag{5}$$

With the dead zone characterized, a software inverse of the dead zone was added to the model in order to approximately linearize the system for identification of plant parameters (see Figure 8). The inverse is $V_{in} = \text{sgn}(V_c)(|V_c| + 3)$, making $V = V_c$ assuming no saturation.

Identification was performed on the system response to a step input of 1 V, representing an applied voltage of 4 V after dead zone compensation. This amplitude was chosen to avoid the saturation regime, so that the system being identified is approximately linear. An MLS identification technique was applied to the resulting data[6, e.g.], and the identified transfer function is shown in (6).

$$\frac{Y(z)}{V(z)} = \frac{0.16572}{z^2 - 1.95833z + 0.95833} \tag{6}$$

To validate this model, experimental and simulation results were compared for a series of square and sinusoidal inputs. The results are shown in Figure 9. Note that the different applied voltages in these open-loop tests result naturally in different motor speeds, and thus the timescales are not the same in each plot. The simulated open-loop system (dashed line) closely matches experimental behaviour (dotted line) for the 1 V amplitude square wave case. This is expected since the model was based on data from a 1 V step input. However, as the input signal amplitude is increased or decreased, or for different waveforms, the model estimate diverges from the actual results. Particularly for low input voltages, the dead zone model underestimates the actual system behaviour. To correct this, the dead zone friction model (5) was modified to include an offset:

$$\begin{aligned} V &= \mathrm{sgn}(V_{sat})[a_0 + \delta(|V_{sat}| - 3)], \quad |V_{sat}| \geq 3 \\ V &= 0, \quad |V_{sat}| < 0 \end{aligned} \tag{7}$$

The identification of the parameters a_0 and δ is detailed in [11]. The solid curves in Figure 9 represent the behaviour for $a_0 = 0.364$ and $\delta = 0.636$. As can be seen from the simulated and experimental plots in Figure 9, the results with the modified dead zone model more accurately reflect the experimental system behaviour for different open-loop voltage waveforms and amplitudes, than the simple dead zone.

Micro-Stage Modelling

This section considers the modelling of the micro stage from the application of the NM70 CTRL signal to the position of the flexure platform. The SMA actuator and associated circuitry form a cascade system as shown in Figure 10. The PWM CTRL signal determines the power applied to the SMA wires. Through Joule heating, this electrical power is converted to temperature which in turn controls the SMA contraction. The hysteretic temperature-contraction relationship is modelled with a Preisach model. It is assumed that the actuator response will not excite flexible modes of the linear flexure stage, so that the flexure platform displacement is equal to that of the actuator.

The first analysis performed is to generate a model representing the inherent hysteresis of the actuator. The Preisach model is adopted and applied using data measured during open-loop heating of the actuator. The model is validated through comparison of simulated and experimental data. An electro-thermal model relating CTRL inputs to wire temperature is then derived and evaluated experimentally.

Hysteresis Model

The Preisach hysteresis model, originally developed for magnetic hysteresis, has also been used to represent smart-material hysteresis, including that observed in SMA [7, 8, e.g.]. In order to develop a micro stage model for simulation and off-line controller design, a Preisach model is identified for the temperature-displacement behaviour of the NanoMuscle actuator. One appealing feature of the Preisach model is that it is invertible and has a computationally-efficient form[9] making it suitable for real-time model inversion for plant linearization.

One implementation of the Preisach model takes the form [9]

$$f(t) = -f^{+} + \sum_{k=1}^{n(t)-1} (f_{M_k,m_k} - f_{M_k,m_{k-1}}) + f_{M_n,m_n} - f_{M_n,m_{n-1}} \tag{8}$$

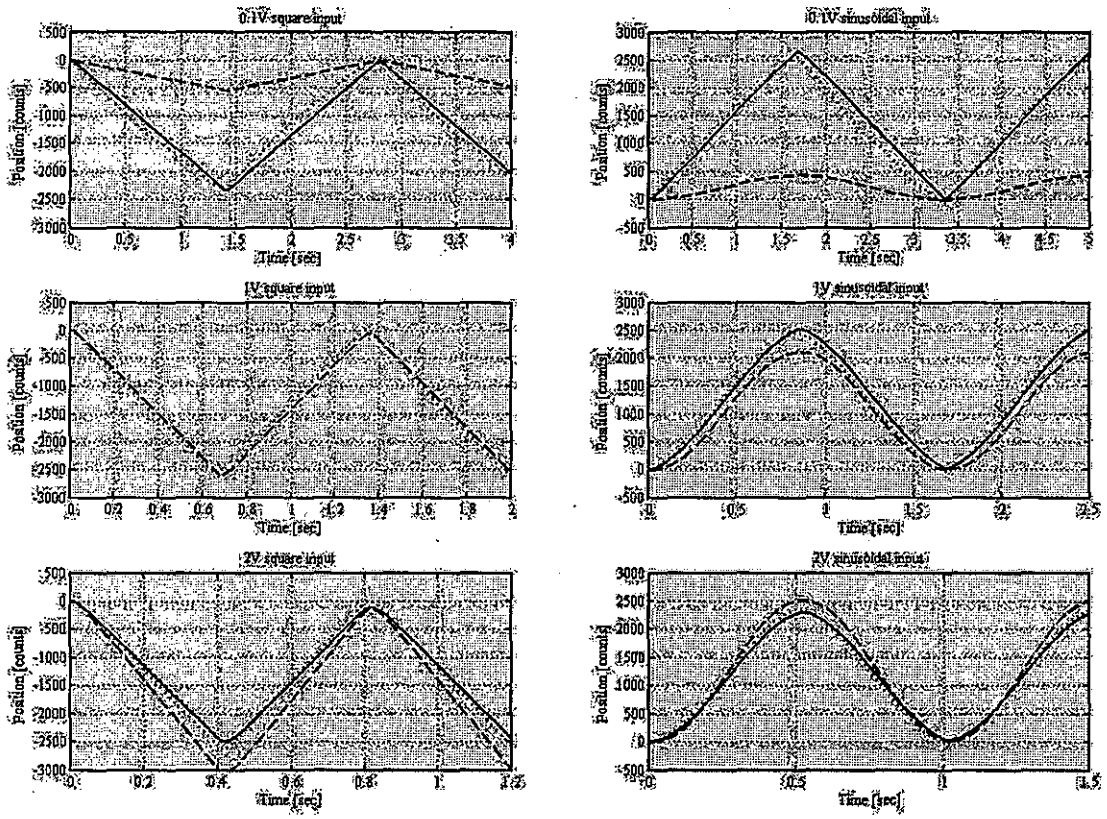

Figure 9: Comparison of experimental (dotted) and simulated output for different open-loop inputs and friction models (dead zone=dashed, modified dead zone=solid)

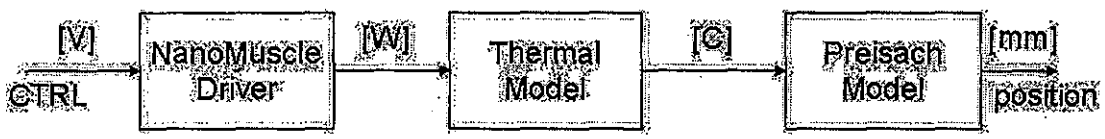

Figure 10: Block Diagram of Actuator Model

where f is the model output, f^+ is a constant, n is the length of a time-varying sequence of past input extrema (the memory of the model), M_k and m_k are values of past input maxima and minima. Terms $f_{a,b}$ are determined through system identification.ma and minima. Terms $f_{a,b}$ are determined through system identification. This process involves the measurement of system output on first-order descending (FOD) curves which are descending branches of the hysteresis curve. They are generated by starting the actuator temperature below the point of negative saturation, heating to a temperature a below positive saturation, and then cooling the actuator while measuring the output at discrete points b over the temperature range. The measured outputs correspond to specific values of $f_{a,b}$. For further details on Preisach model identification and properties, the reader is referred to [9].

To identify the data required for the NanoMuscle Preisach model, a series of FOD curves were generated using a programmable kiln to heat the actuator, thus providing direct control of the temperature. The setup of the kiln is shown in Figure 11a. Current controlled by a solid-state relay generates heating through a resistive heating element in the kiln. The temperature of the NanoMuscle is measured using a thermocouple fixed to the top plate of the actuator. The actuator is mass-biased with a 30 gram weight, and displacement is measured using an optical encoder with a linear resolution of approximately 14 μm. The temperature is monitored, and the relay contactor of the kiln controlled, by a micro-controller via a LabView interface on a PC.

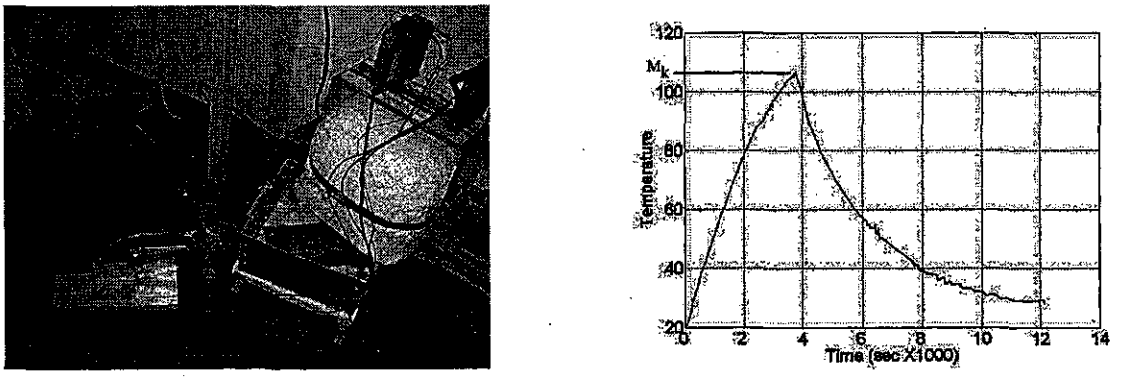

(a) (b)

Figure 11: Preisach Identification Setup using the (a) Kiln and (b) Sample Temperature Profile

Using the kiln test bed, the NanoMuscle was repeatedly heated to different maximum temperatures M_k, then cooled back down to ambient temperature, generating FOD curves. An example temperature profile that was measured from the actuator is shown in Figure 11b. With each heating cycle, the temperature peak M_k was decreased. As the actuator cooled, displacement measurements were taken at decreasing values of temperature, m_k, and assigned to FOD data point f_{M_k,m_k}. The resulting family of FOD curves is shown in Figure 12a. To test the validity of the resulting Preisach model, (8) was implemented in Matlab using data from the measured FOD curves. A new series of temperature profiles from independent kiln tests were simulated and the results compared favourably with experimental data, as shown in Figure 12b.

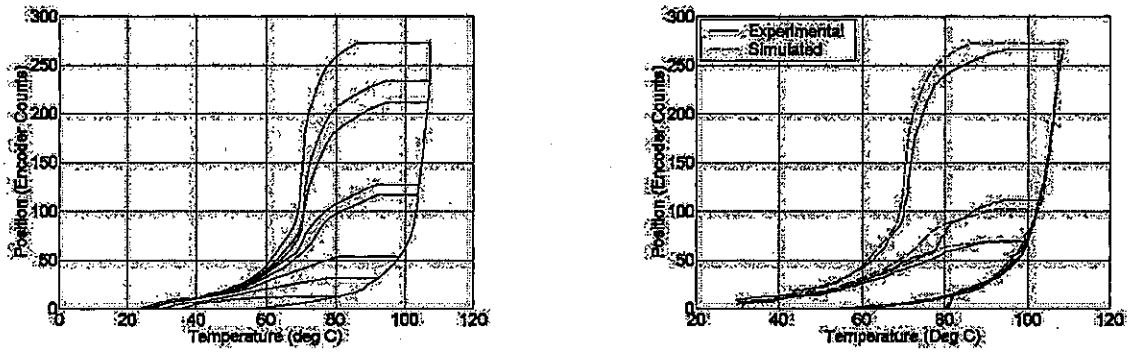

(a) (b)

Figure 12: Preisach Model (a) Experimental FOD data and (b) Validation

Electro-Thermal Model

Since the intermediate signal is not available without modifying the NanoMuscle, the first two blocks of Figure 10 must be modelled together. The result represents the relationship between the input CTRL signal and the wire temperature. This is complicated by the inability to accurately measure the temperature of the 50 μm diameter wire used in the NanoMuscle actuator, and the proprietary nature of the control circuitry.

A method of inferring temperature from actuator position was developed, which makes use of the data gathered during Preisach identification of the temperature-position behaviour. With the actuator starting from consistent initial conditions (room temperature, constant load), open-loop step inputs of various magnitudes were applied to the CTRL signal, held until the position reached steady-state (for 300 seconds), then removed. The position response was recorded over both the heating and cooling cycles. Figure 13a shows the heating portion of the response. For each CTRL voltage from 1.5 V to 1.8 V, the solid lines represent the average of the three responses shown in dashed lines.

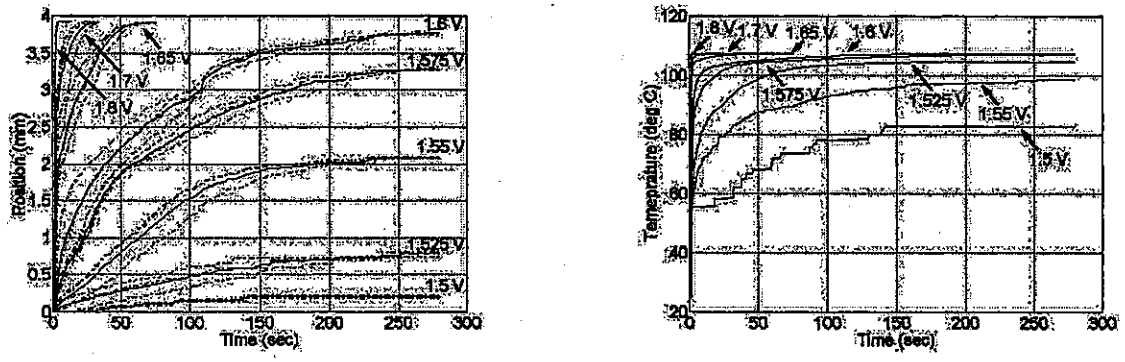

(a) (b)

Figure 13: Micro-Stage (a) Position and (b) Inferred Temperature Response for Varying CTRL Step Input Voltages

Assuming the temperature in response to a step CTRL input is monotonic, each step input of varying magnitude traces out a different FOD curve in the temperature-position relation. During the first 300 seconds, the actuator follows the ascending branch of the major hysteresis loop, to a point determined by the test input magnitude. During cooling, a descending branch is followed. FOD data can therefore be used to infer wire temperature based on actuator position. This inference procedure only works if the actuator starts in the full-martensite condition. Since transformation temperatures and hence contraction are stress-dependent, it also assumes that the actuator is under the same loading conditions as used during FOD curve identification. Figure 13b shows the temperature response inferred from each of the averaged position curves of Figure 13a. Figure 14 shows the inferred cooling response when the CTRL input is removed and the SMA wire cools passively via convection to the environment. For CTRL steps greater than 1.575 V the steady-state temperature, and hence the cooling curves, are the same.

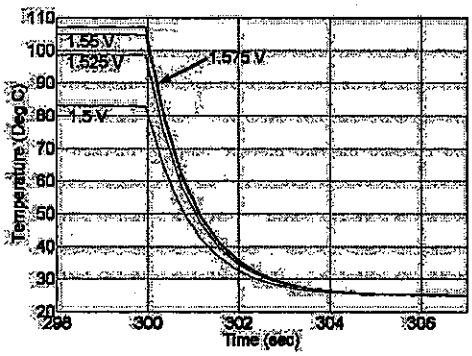

Figure 14: Micro-Stage Cooling Inferred Temperature Response for Varying CTRL Step Input Voltages

The cooling curves decay exponentially with a time constant of $\tau \approx 1\,\mathrm{s}$. This illustrates the limited bandwidth available from the micro-stage actuator. For full extension (4 mm travel), cooling takes approximately 4 s resulting in a maximum bandwidth of 0.25 Hz. For a more detailed investigation of the NanoMuscle bandwidth and the effects of repeated cycling, see [12].

To account for the non-linearities present in the NanoMuscle driver circuitry, the overall heating was modelled as a nonlinear gain $\phi(\mathrm{CTRL})$ followed by a linear transfer function which incorporates the heating dynamics, $\Theta_h(s)$. The driver circuitry has no effect on cooling, and a standard first-order cooling model, $\Theta_c(s)$, was used.

Figure 15 shows the resulting heating model validation. It can be seen that the steady-state match is quite good, but that there is significant dynamic error still in the model. Figure 16 compares the combined heating, cooling, and Preisach models in simulation with experimental data for CTRL step inputs of various magnitudes. Again, steady-state matching is good but there remains significant transient error. As a result, the model was not considered adequate for model-based controller design. The details of the heating and cooling models are omitted here, but can be found in [13].

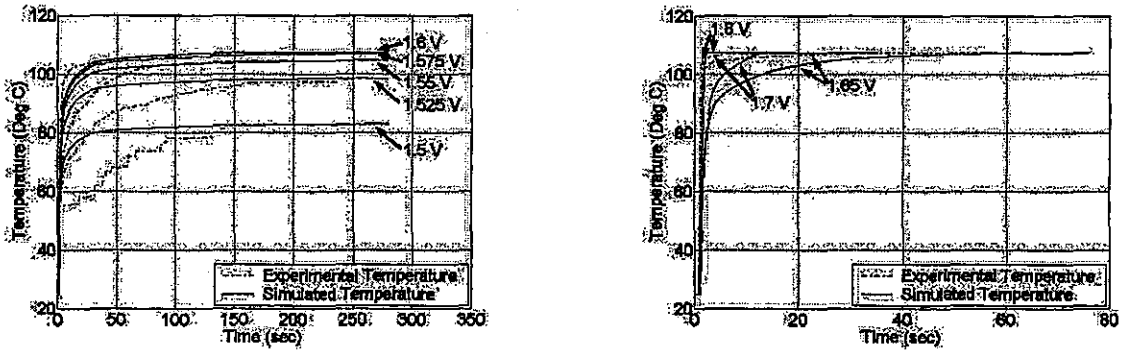

(a) (b)

Figure 15: Weighted Heating Model Validation Temperature Response for (a) 1.5 - 1.6 V and (b) 1.65 - 1.8 V Step Input

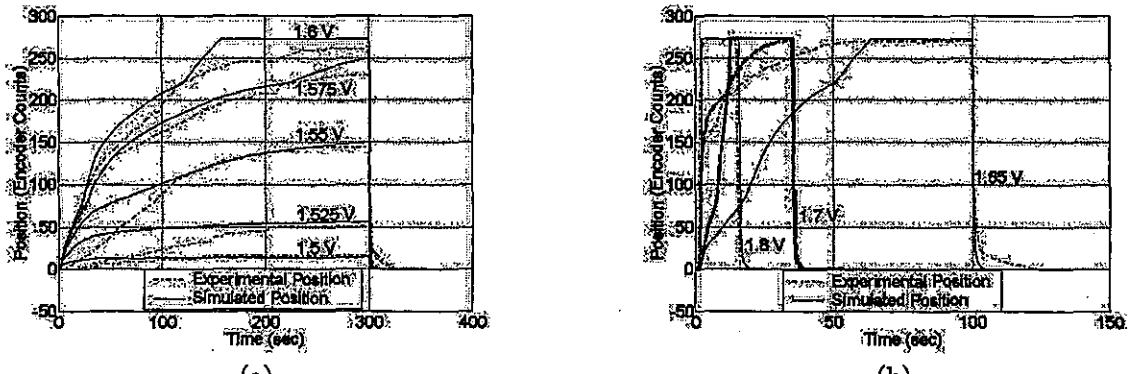

(a) (b)

Figure 16: Complete SMA Actuator Model Validation for (a) 1.5 - 1.6 V and (b) 1.65 - 1.8 V Step Input

CONTROL

This section describes the control strategy implemented on the macro-micro manipulator. The envisaged application involves the macro stage moving to a series of specified locations and the micro stage performing local tasks involving relative motion at each location, for example for visual inspection. Controllers are developed individually for the macro and micro stages and then combined for evaluation in the context of this overall task.

Macro-Stage Control

In this section, a controller is developed for the macro stage using the simulation model developed in the Macro-Stage Modelling section. The controller performance is compared experimentally to a PID controller developed and tuned directly on the prototype. The result emphasizes the benefit of having a good nonlinear simulation model.

Benchmark PID Controller

Figure 17 shows the control effort and step response for a step input command to the macro stage, using a PID controller tuned experimentally with goals of fast settling time, low overshoot and low steady-state error.

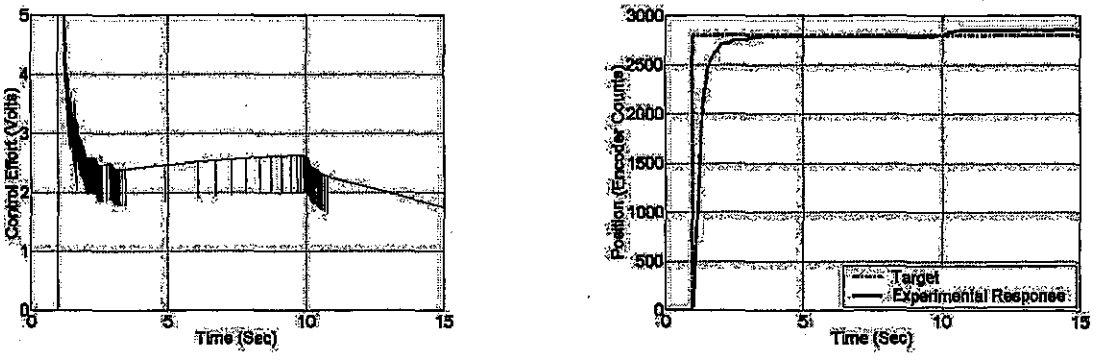

(a) (b)

Figure 17: Macro-Stage (a) Controller Output and (b) System Response using Benchmark PID Controller

As seen in Figure 17b, the rise time is fairly good but the integral control is unable to eliminate the steady-state error, due to friction. A constant error due to friction contributes to an increasing integral control effort, as can be seen in Figure 17a from 4 to 10 seconds. When the control does finally overcome friction, the carriage overshoots and sticks again. Interpretation of the control effort provides some insight into the system behaviour. The negative spikes in Figure 17a reflect the effect of the derivative control and occur when the error changes discretely as a result of carriage motion. Those portions of the control signal which ramp with constant slope represent periods of no carriage motion. As can be seen, beyond about 11 seconds the carriage has ceased to move, and will remain motionless until the control voltage drops to approximately -3 V, due to stiction. Eventually, this results in a limit cycle behaviour typical of integrator systems with friction.

Nonlinear Controller Design

To replace the PID controller, a nonlinear PD controller was designed in simulation using the model developed in the Macro-Stage Modelling section. Since the PD controller has a dead zone inverse nonlinearity at the output to compensate for drive friction, it is important to avoid overshoot which could induce chatter and instability in the system. The controller damping ratio and phase margin frequency were tuned in simulation to produce a good response time while avoiding overshoot.

The linear (PD) portion of the tuned controller is shown in (9). The output of this linear controller u is modified to compensate for the friction identified in the macro-stage drive, and the resulting control signal $u' = u + 3\,\mathrm{sgn}(u)$ is applied to the experimental system. The experimental and simulation results for a decaying square wave input are compared in Figure 18. Aside from some slight mismatch at high displacements, the experimental and modelled responses match well, indicating an accurate model. The response time is better than that achieved with the experimentally-tuned PID controller. As can be seen in Figure 19, the steady-state error is eliminated by the controller "nudging" the carriage toward the target. Note the reaction of the control signal as the error is reduced: with each movement of the carriage the derivative change is penalized, causing the control to appear to chatter due to the dead zone inverse friction compensation. The change is momentary, however, and has no effect on the actual position. The controller continues to reduce the steady-state error to zero with no overshoot. This same behaviour is reproduced at each step of decreasing amplitude, with steady-state error reduced to zero each time.

$$\frac{U}{E} = \frac{0.0124593z + 0.0112178}{z} \tag{9}$$

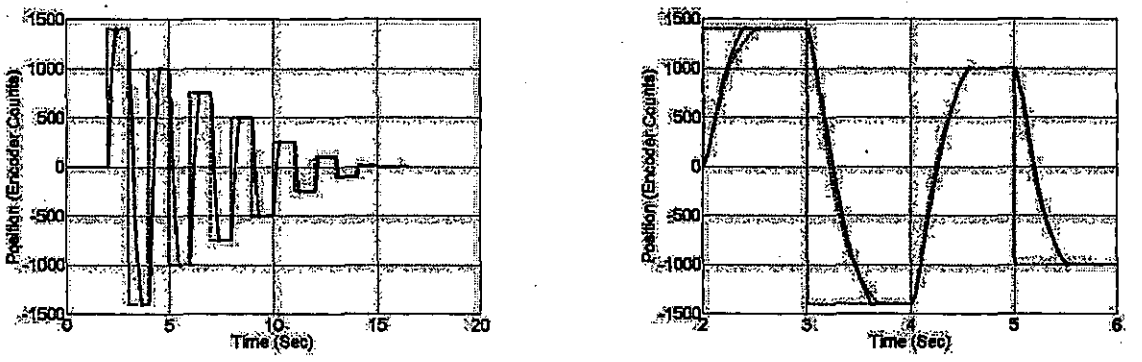

(a) (b)

Figure 18: (a) Full and (b) Zoomed Comparison of Experimental and Simulated Closed Loop Responses with Tuned Nonlinear Controller. Legend: Target (Dash-dot), Simulated (Solid), Experimental (Dotted) Response

Closed Loop Micro-Stage Control

The model developed in of the micro stage provided only qualitative representation of the dynamic behaviour. The controller for the micro stage therefore had to be designed and tuned experimentally on the prototype. Past work has shown that PI controllers perform well on SMA actuators[14],

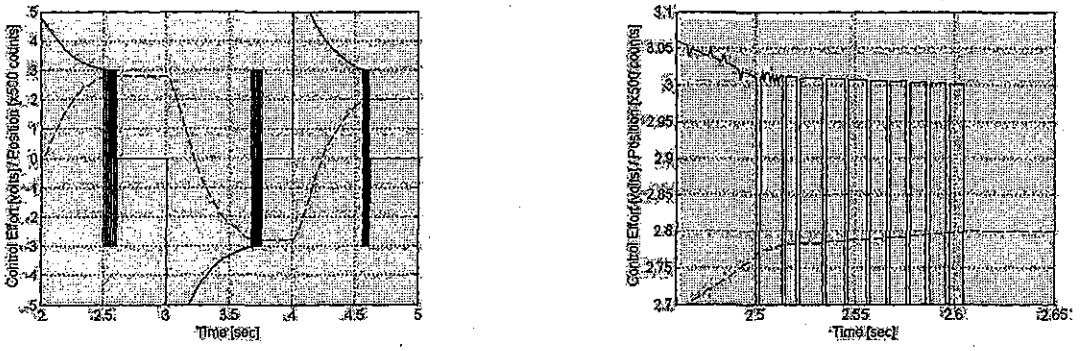

(a) (b)

Figure 19: (a) Full and (b) Zoomed Plot of Experimental Position (scaled) and Control Effort. Legend: Control Effort (Solid), Scaled Position (Dashed)

so this controller structure was chosen. In order to mitigate the problems of integrator windup associated with saturation nonlinearities in the NanoMuscle, the classic anti-windup technique of [15] was implemented. The final micro stage controller structure is shown in Figure 20.

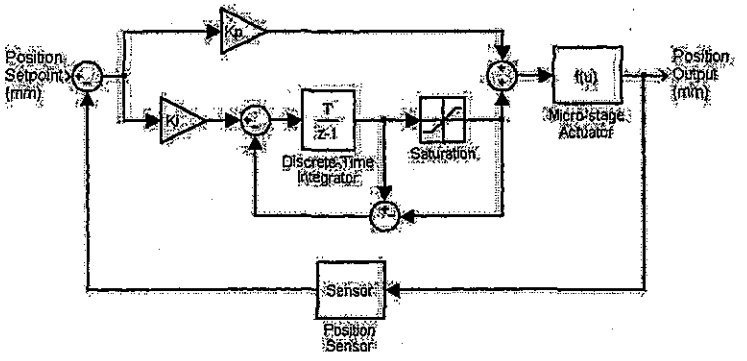

Figure 20: Block Diagram of Micro Stage Using PI Control with Anti-Windup

The lower limit of the anti-windup saturation is set to 1.3 V, since CTRL signals below this value have no effect on the actuator. The upper limit is set to 1.9 V. The tuned gains were $K_p = 3$, $K_i = 30$, and the controller was implemented and tested on the micro stage actuator with a sequential step input. The result is shown in Figure 21. As can be seen, the controller performs well, producing little overshoot or steady-state error, and a settling time of approximately 250 ms in contraction for 50% travel, and 1 second for extension. As can be seen in Figure 21b, the 5 μm target accuracy for the micro stage has been met. Note that position measurements for the plots shown were taken from an Agilent laser measurement system. The Hall effect sensors on the flexure stage were used for control feedback.

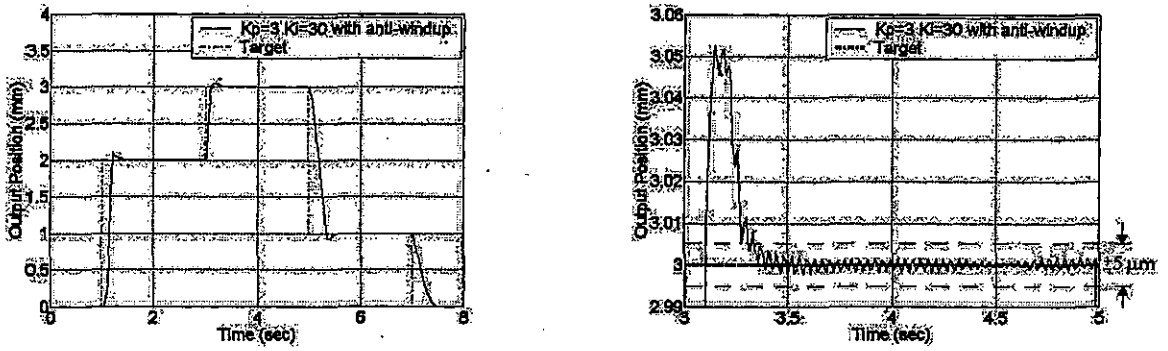

(a) (b)

Figure 21: Sequential Step Input (a) Full and (b) Zoomed Response of Micro Stage with PI Control with Anti-Windup. ($K_p = 3$ and $K_i = K_{aw} = 30$)

Integrated Control

Here, the controllers are combined on the macro-micro prototype and tested experimentally. A task is simulated where the macro stage performs a series of step movements throughout its workspace, with the micro stage carrying out simulated operations at each location in the macro workspace. Though the position feedback measurement is provided by a cost-effective Hall effect sensor, an Agilent laser measurement system is used to independently measure displacement for calibration and testing purposes. The test input consists of a decaying square wave for the macro stage and a sequential step for the micro stage after each macro movement. The goal is to have the macro stage reach its set point and then allow the micro stage to operate with precision within a small area relative to the steady-state macro-stage position. The resulting response is shown in Figure 22. Figure 22a includes the macro-stage reference signal; micro-stage motion is visible at each location of the macro stage. Figure 22b shows the micro stage response after the second macro-stage step, along with the shifted micro stage reference. Micro-stage motion begins at 18 seconds, after the macro stage has settled.

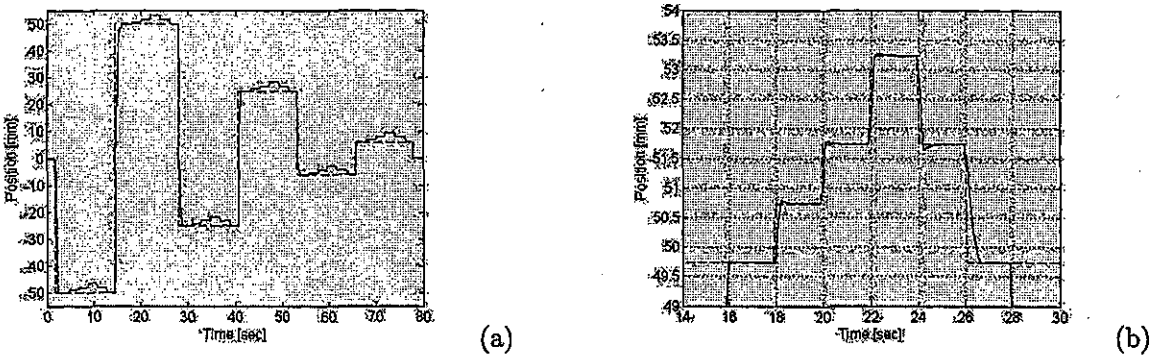

(a) (b)

Figure 22: (a) Full and (b) Zoomed View of Integrated System Response

CONCLUSIONS

The developed experimental system comprises a modified printer to provide long range, macro scale linear motion (approximately 200 mm range and 50 μm precision) and a micro scale system (approximately 4 mm range and 5 μm precision) that uses a NanoMuscle SMA actuator. Monitoring and computer control is achieved by Simulink via a MultiQ-3 data acquisition board manufactured by Quanser Consulting.

For the macro stage, a simple discontinuous dead zone was used to model and compensate for friction. The resulting approximately linear system was modelled using a modified least squares approach. Despite the simplicity of the friction model, the experimental and simulated behaviour show a good match for different input waveforms of various amplitudes. The model was then used to develop a tuned nonlinear PD controller off line employing a linearizing dead zone inverse. The model was implemented experimentally and shown to produce excellent results. Of particular interest is the way in which the friction linearization and combination of proportional and derivative control work together to eliminate steady-state error without overshoot or integral control.

A Preisach model was identified for the NanoMuscle actuator, which provided good qualitative representation of the temperature-displacement behaviour of the actuator. However, difficulties in temperature measurement and the proprietary nature of the NanoMuscle control circuitry made it difficult to create a good model for the overall system. Closed loop control for the micro stage was implemented through an experimentally-tuned PI controller with anti-windup. The controller provided excellent performance when integrated with the macro stage.

The experimental prototype exceeded the goal of 5μm relative positioning accuracy, using low-cost components. The overall cost of the prototype, not including data acquisition hardware and amplifiers, was approximately $250, including manufacturing of custom parts like the flexure guide. While the micro-stage bandwidth is limited, the success of the prototype provides us with a platform to study a number of further issues associated with low-cost positioning on the micron scale. Future work on this system will include

- an assessment of coupling in the system and vibration induced in the micro stage from macro-stage motion,
- comparison of the simple model implemented here with additional friction models,
- continued investigation of the NanoMuscle model, and
- addition of a CCD camera to the flexure platform to enable fiducial recognition and inspection.

References

[1] Burleigh Instruments Inc. *Nanopositioning Instrumentation Price List.* Burleigh Instruments, Inc., New York, 2000.

[2] EXFO. EXFO IW-800 Series–Inchworm Motors. http://www.exfo.com/en/products/ProductsView.asp?Product=187 (current Aug 31, 2006).

[3] NanoMuscle Inc. 70 Gram HS/HE Linear Actuator Manual. Note: NanoMuscle has ceased operations and the technology has been acquired by MIGA Motor Company. Some docu-

mentation is available at http://www.migamotors.com/NM70_motor_DI.pdf (current Aug 27, 2006).

[4] S.T. Smith and D.G. Chetwynd. *Foundations of Ultraprecision Mechanism Design.* Gordon and Breach Science, Pennsylvania, 1992.

[5] Honeywell International Inc. Interactive Catalog - Honeywell Sensing and Control. http://catalog.sensing.honeywell.com/datasheet.asp?FAM=Accessory&PN=103MG5 (current Aug 31, 2006).

[6] L. Ljung. *System Identification: Theory for the User.* Prentice-Hall, New Jersey, 1987.

[7] R.B. Gorbet, D.W.L. Wang and K.A. Morris. Preisach Model Identification of a Two-Wire SMA Actuator. *Proceedings of the 1998 IEEE International Conference on Robotics and Automation*, 3:2161–2167, 1998.

[8] D. Hughes and J.T. Wen. Preisach Modeling of Piezoceramic and Shape Memory Alloy Hysteresis. *IEEE International Conference on Control Applications*, pages 1086–1091, 1995.

[9] I.D. Mayergoyz. *Mathematical Model of Hysteresis.* Springer-Verlag, New York, 1991.

[10] M.W. Spong and M. Vidyasagar. *Robot Dynamics and Control.* John Wiley & Sons, Toronto, 1989.

[11] E. Ho and R.B. Gorbet. Nonlinear Macro Drive Model Identification for a Macro-Micro Positioning System. *3rd IFAC Symposium on Mechatronic Systems*, 2004. Sydney, Australia.

[12] E. Ho and R.B. Gorbet. Potential of the NanoMuscle SMA Actuator for Fine Position Control. *3rd Annual CanSmart International Workshop on Smart Materials and Structures*, pages 87–96, 2003. Montreal, QC.

[13] E.M.T. Ho. Linear Macro-Micro Positioning System Using a Shape Memory Alloy Actuator. Master's thesis, University of Waterloo, Waterloo, Ontario, 2004.

[14] R.B. Gorbet and D.W.L. Wang. A Dissipativity Approach to Stability of a Shape Memory Alloy Position Control System. *IEEE Transactions on Control Systems Technology*, 6(4):554–562, 1998.

[15] G.C. Goodwin, S.F. Graebe and M.E. Salgado. *Control System Design.* Prentice-Hall, New Jersey, 2001.